HHS Public Access

Author manuscript

Atherosclerosis. Author manuscript; available in PMC 2022 January 22.

Published in final edited form as:

Atherosclerosis. 2021 March ; 320: 98–104. doi:10.1016/j.atherosclerosis.2020.12.018.

Spatial relationships among hemodynamic, anatomic, and biochemical plaque characteristics in patients with coronary artery disease

Anubodh S. Varshney[a,b], **Ahmet U. Coskun**[c], **Gerasimos Siasos**[d], **Charles C. Maynard**[e], **Zhongyue Pu**[a,b], **Kevin J. Croce**[a,b], **Nicholas V. Cefalo**[a], **Michelle A. Cormier**[a], **Dimitris Fotiadis**[f], **Kostas Stefanou**[f], **Michail I. Papafaklis**[f], **Lampros Michalis**[f], **Stacie VanOosterhout**[g], **Abbey Mulder**[g], **Ryan D. Madder**[g], **Peter H. Stone**[a,b,*]

[a]Brigham and Women's Hospital Heart & Vascular Center, Boston, MA, USA

[b]Harvard Medical School, Boston, MA, USA

[c]Department of Mechanical and Industrial Engineering, Northeastern University, Boston, MA, USA

[d]1st Department of Cardiology, National and Kapodistrian University of Athens, School of Medicine, Hippokration General Hospital, Athens, Greece

[e]University of Washington, Seattle, WA, USA

[f]Faculty of Medicine, University of Ioannina, Ioannina, Greece

[g]Frederik Meijer Heart & Vascular Institute, Spectrum Health, Grand Rapids, MI, USA

Abstract

Background and aims: We aimed to characterize the spatial proximity of plaque destabilizing features local endothelial shear stress (ESS), minimal luminal area (MLA), plaque burden (PB), and near-infrared spectroscopy (NIRS) lipid signal in high- *vs.* low-risk plaques.

*Corresponding author. Division of Cardiovascular Medicine, Brigham and Women's Hospital, Harvard Medical School, 75 Francis St, Boston, MA, 02115, USA. pstone@bwh.harvard.edu (P.H. Stone).

Author contributions

Anubodh S. Varshney, Ahmet U. Coskun, Gerasimos Siasos, Charles C. Maynard, Zhongyue Pu, Kevin J. Croce, Nicholas V. Cefalo, Michelle A. Cormier, Dimitris Fotiadis, Kostas Stefanou, Michail I. Papafaklis, Lampros Michalis, Stacie VanOosterhout, Abbey Mulder, Ryan D. Madder, Peter H. Stone:

Substantial contributions to the conception or design of the work.

Acquisition, analysis, or interpretation of data for the work.

Drafting the work and/or revising it critically for important intellectual content.

Final approval of the version to be published.

Agreement to be accountable for all aspects of the work in ensuring that questions related to the accuracy or integrity of any part of the work are appropriately investigated and resolved.

Declaration of competing interest

The authors declare the following financial interests/personal relationships which may be considered as potential competing interests: Ryan D. Madder: has received research support and speaker honoraria from InfraRedx and serves on the advisory board of SpectraWave.

Peter H. Stone: has received research support from InfraRedx.

Appendix A. Supplementary data

Supplementary data to this article can be found online at https://doi.org/10.1016/j.atherosclerosis.2020.12.018.

Methods: Coronary arteries imaged with angiography and NIRS-intravascular ultrasound (IVUS) underwent 3D reconstruction and computational fluid dynamics calculations of local ESS. ESS, PB, MLA, and lipid core burden index (LCBI), for each 3-mm arterial segment were obtained in arteries with large lipid-rich plaque (LRP) *vs.* arteries with smaller LRP. The locations of the MLA, minimum ESS (minESS), maximum ESS (maxESS), maximum PB (maxPB), and maximum LCBI in a 4-mm segment ($maxLCBI_{4mm}$) were determined along the length of each plaque.

Results: The spatial distributions of minESS, maxESS, maxPB, and $maxLCBI_{4mm}$, in reference to the MLA, were significantly heterogeneous within and between each variable. The location of $maxLCBI_{4mm}$ was spatially discordant from sites of the MLA ($p<0.0001$), minESS ($p = 0.003$), and maxESS ($p = 0.003$) in arteries with large LRP ($maxLCBI_{4mm} \geq 400$) and non-large LRP. Large LRP arteries had higher maxESS (9.31 ± 4.78 *vs.* 6.32 ± 5.54 Pa; $p = 0.023$), lower minESS (0.41 ± 0.16 *vs.* 0.61 ± 0.26 Pa; $p = 0.007$), smaller MLA (3.54 ± 1.22 *vs.* 5.14 ± 2.65 mm^2; $p = 0.002$), and larger maxPB (70.64 ± 9.95% *vs.* 56.70 ± 13.34%, $p<0.001$) compared with non-large LRP arteries.

Conclusions: There is significant spatial heterogeneity of destabilizing plaque features along the course of both large and non-large LRPs. Large LRPs exhibit significantly more abnormal destabilizing plaque features than non-large LRPs. Prospective, longitudinal studies are required to determine which patterns of heterogeneous destabilizing features act synergistically to cause plaque destabilization.

Graphical Abstract

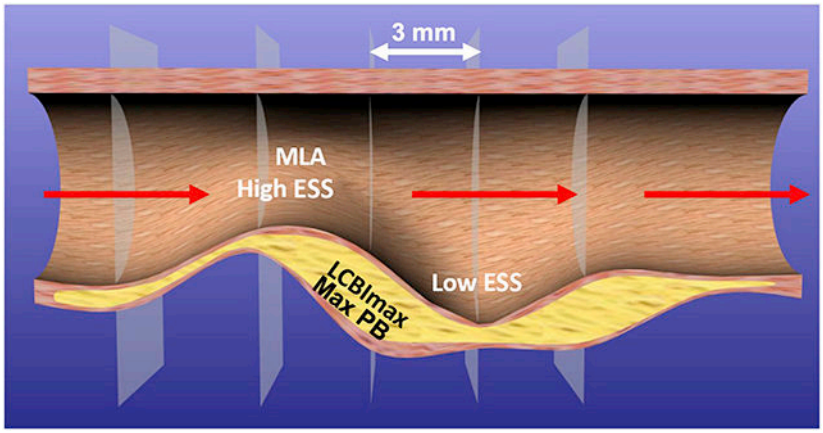

Keywords

Atherosclerosis; Coronary artery disease; Intravascular ultrasound; Endothelial shear stress; Near infrared spectroscopy; Vulnerable plaque

1. Introduction

Coronary artery disease (CAD) remains the leading cause of death globally [1]. Identifying patients and coronary plaques at high risk of major adverse cardiovascular events (MACE) may augment the efficacy of existing preventive therapies and aid in the

development of future pre-emptive treatment strategies. Despite systemic vascular exposure to cardiovascular risk factors (e.g. smoking, hyperlipidemia), individual coronary arterial plaques have heterogeneous natural history trajectories within the same patient. Local anatomic, hemodynamic, and biochemical factors are important determinants of plaque progression, regression, and quiescence [2,3].

Plaques at increased risk of causing MACE are anatomically characterized by plaque burden (PB) ≥70%, minimal luminal area (MLA) ≤ 4 mm^2, and thin-cap fibroatheroma (TCFA) morphology [3-6]. However, the positive predictive value of these anatomic features alone is insufficient to guide clinical decision-making. Low local endothelial shear stress (ESS) is a potent pro-inflammatory, pro-atherogenic hemodynamic and biomechanical stimulus that is associated with plaque development and progression [7-9]. When added to PB, MLA, and TCFA morphology, low ESS confers incremental risk of need for coronary revascularization [10] and MACE [11]. High ESS may also be responsible for plaque destabilization leading to acute myocardial infarction (MI) [12,13].

Additionally, the presence of large lipid cores within plaques has been associated with MACE. Plaque lipid content can be assessed with near-infrared spectroscopy (NIRS), which detects areas where lipid is likely to be present and provides a quantitative estimate of the amount of lipid present as a lipid-core burden index (LCBI). Large lipid-rich plaques (LRP) have been shown to be present at culprit sites of ST-elevation myocardial infarction (STEMI), non-STEMI, and unstable angina in cross-sectional studies [14,15], and prospective registry studies indicate that a maximum LCBI within a 4-mm coronary arterial section ($maxLCBI_{4mm}$) ≥ 400 reliably discriminates culprit from non-culprit sites [15,16]. Additionally, $maxLCBI_{4mm}$ ≥ 400 in non-culprit arteries has been shown to be associated with increased risk for future MACE [17].

Though local ESS, PB, MLA, and NIRS lipid signal have been studied in isolation in various patient populations, the spatial relationships among these hemodynamic, anatomic, and biochemical variables are currently unknown, as is the degree to which they act synergistically with one another to promote plaque progression and/or destabilization. It is also unknown whether large LRPs are most prone to destabilize at a particular location along the course of the plaque, such as the $maxLCBI_{4mm}$ or MLA. Recent studies underscore the marked heterogeneity in morphology, constituents, and biomechanical influences along the longitudinal course of an individual plaque [18,19], heterogeneous localization of the site of plaque destabilization [11,18-20], and the adverse prognostic significance of such heterogeneity [21]. Understanding the complex interplay among these plaque elements may facilitate further insights into the multifaceted vascular biology of plaque progression and destabilization and allow for more accurate identification of high-risk coronary plaques likely to cause new MACE. The purpose of this study, therefore, was to explore how destabilizing features of local ESS patterns, PB, MLA, and NIRS lipid signal spatially relate to one another, and whether the spatial relationships among these variables differ in arteries with high-risk large LRP (defined as $maxLCBI_{4mm}$ ≥ 400) *vs.* arteries with non-large LRP (defined as $maxLCBI_{4mm}$ < 400).

2. Patients and methods

2.1. Study population

This study analyzed patients from the Spectrum NIRS-IVUS Registry (NCT01694368), which is a single-center, observational registry of prospectively enrolled patients undergoing invasive angiography and combined NIRS-IVUS imaging. As previously described, inclusion criteria for participation in the registry are age ≥18, referral to the catheterization laboratory for clinically-indicated invasive coronary angiography and/or percutaneous coronary intervention (PCI), ≥1 severe coronary artery stenosis by invasive angiography and PCI planned for definitive treatment or found to have ≥1 intermediate coronary artery stenosis and IVUS planned for lesion assessment, and performance of NIRS-IVUS imaging within at least one coronary artery [22]. The study complies with the Declaration of Helsinki, was approved by the Institutional Review Board of Spectrum Health, and all participants provided written informed consent.

In order to compare ESS, MLA, PB, and NIRS lipid signal in arteries with and without large LRP, arteries from patients in the registry were randomly selected for inclusion in this analysis based on the presence or absence of a $maxLCBI_{4mm} \geq 400$ in a non-culprit segment. All arteries required at least 10 mm of interpretable NIRS-IVUS data for inclusion in this analysis. Arteries that had undergone PCI prior to NIRS-IVUS imaging were excluded. Additional exclusion criteria included the presence of artifact or poor image quality limiting NIRS-IVUS interpretation. Arteries with at least one $maxLCBI_{4mm} \geq 400$ in a non-culprit segment and arteries without a $maxLCBI_{4mm} \geq 400$ were randomly selected for inclusion and underwent core laboratory analysis by two imaging analysts.

2.2. Core laboratory analysis

NIRS-IVUS chemograms and $maxLCBI_{4mm}$ values were obtained for culprit and non-culprit arteries. Local ESS values were obtained using validated vascular profiling techniques, in which biplane coronary angiography and IVUS images are used to reconstruct the coronary artery lumen and perform computational fluid dynamics (CFD) calculations [10]. Side branches were excluded from CFD calculations. Arteries that could not undergo full vascular profiling due to technical reasons were excluded. Customized software was used to merge coronary angiographic and IVUS centerlines in order to create 3-dimensional reconstructions of coronary arteries [23]. Each artery was divided into 3-mm segments, and the minimum ESS (minESS), maximum ESS (maxESS), maximum PB (maxPB), and minimum lumen area (MLA) for each segment was obtained. The minESS and maxESS for each segment were determined in a moving window of 90° arcs around the circumference of the vessel. The maximum LCBI value was obtained for each 4 mm segment as this is primary output of the NIRS-IVUS device and the $maxLCBI_{4mm}$ is the measure used in previous studies evaluating the prognostic value of LCBI. Since there is only one $maxLCBI_{4mm}$ per artery, identifying this measure within a 4-mm or 3-mm segment would not result in a difference in value or location.

The segment locations of minESS, maxESS, maxPB, MLA, and $maxLCBI_{4mm}$ were determined for each artery. These locations were then related to each other spatially.

Variables were categorized as spatially concordant if they were located at the same 3-mm segment or within one 3-mm segment of each other, since this degree of spatial proximity may pathobiologically enable and promote synergy among plaque features. Otherwise, variables were categorized as spatially discordant.

2.3. Statistical analysis

Continuous variables are reported as means and standard deviations and categorical variables as numbers and percentages. The Chi-square statistic was used to compare spatial heterogeneity between prognostic variables, and the binomial test to determine if the distribution of concordance and discordance differed for MLA, maxESS, and minESS. We also used linear regression to compare large and non-large LRP arteries for continuous measures such as $maxLCBI_{4mm}$, ESS, MLA, and % area of a certain ESS threshold. *P* values were adjusted for potential correlated error due to multiple observations per patient with the Huber-White Sandwich Estimator. We employed logistic regression to compare large and non-large LRP with concordance status for MLA, maxESS, and minESS. *p* values were adjusted for potential correlated error with the Huber-White Sandwich Estimator. All analyses were performed with STATA software version 15 (Stata Corporation, College Station, Texas, U.S.A.).

3. Results

3.1. Patient characteristics

From a total of 97 arteries from 63 patients who underwent coronary angiography with concurrent NIRS-IVUS imaging, 60 arteries (27 large LRP and 33 non-large LRP) were analyzed from 49 patients (Fig. 1). Most arteries that were excluded had less than 10 mm NIRS-IVUS pullback, imaging artifact, and/or poor image quality. The mean age was 63 ± 10.0 years and 67% (33/49) of patients were male. An acute coronary syndrome represented the indication for invasive angiography in 35% (17/49) of patients and 32% (19/60) of plaques. A total of 58% (11/19) of these acute coronary syndrome plaques were derived from culprit arteries. Patient characteristics are summarized in Table 1.

3.2. Spatial relationship of local ESS, maxPB, and $maxLCBI_{4mm}$ relative to site of MLA

Arteries in which maxESS (n = 3) or minESS (n = 21) was greater than 15 mm from the site of the MLA were excluded from this analysis because ESS beyond that distance was considered unlikely to be germane as a destabilizing influence for that plaque. The maxESS location was most frequently at the site of the MLA (28/57, 49.1%) or 3 mm proximal to the site of the MLA (16/57, 28.1%), and maxPB was most frequently at the site of the MLA (47%). In contrast, minESS was either proximal (18/39, 46.2%) or distal (21/39, 54.0%) to the site of the MLA but not found at the site of the MLA in any arteries. The $maxLCBI_{4mm}$ was proximal to (14/37, 37.8%), distal to (11/37, 29.7%), or at the site of (12/37, 32.4%) the MLA in similar proportions.

Within each prognostic variable, there was significant spatial heterogeneity along the course of each plaque in reference to the MLA by binomial test: minESS ($p < 0.0001$), maxESS ($p < 0.0001$), maxPB ($p = 0.002$), and $LCBImax_{4mm}$ ($p<0.0001$). Similarly, there was

significant spatial heterogeneity between prognostic variables along the course of each plaque by Chi-square: minESS *vs.* maxESS, $p < 0.0001$; minESS *vs.* maxPB, $p < 0.0001$; minESS *vs.* $maxLCBI_{4mm}$, $p < 0.0001$; maxESS vs maxPB, $p = 0.048$; maxESS *vs.* $maxLCBI_{4mm}$, $p < 0.0001$; maxPB *vs.* $maxLCBI_{4mm}$, $p = 0.005$ (Fig. 2).

3.3. Characteristics of large LRP and non-large LRP arteries

The overall characteristics of large and non-large LRP arteries are summarized in Table 2. By definition, $maxLCBI_{4mm}$ was higher in large LRP arteries compared with non-large LRP arteries (610 ± 161.4 *vs.* 200.1 ± 109.5; $p < 0.0001$). The minESS (0.41 ± 0.16 *vs.* 0.61 ± 0.26 Pa; $p = 0.007$) and MLA (3.54 ± 1.22 *vs.* 5.14 ± 2.65 mm^2; $p = 0.002$) were lower and the maxPB (70.94 ± 9.95% *vs.* 56.70 ± 13.34%, $p < 0.0001$) and maxESS (9.31 ± 4.78 *vs.* 6.32 ± 5.54 Pa; $p = 0.023$) were higher in large LRP arteries compared with non-large LRP arteries. The percentage of arterial area with low ESS <1.0 Pa was similar in both large and non-large LRP arteries (20.9% ± 13.8% *vs.* 26.0% ± 24.9%; $p = 0.86$), while the percentage of arterial area with high ESS >3.5 Pa was higher in large LRP arteries compared with non-large LRP arteries (35.5% ± 21.9% *vs.* 19.4% ± 23.8% $p = 0.028$). The distribution of different magnitudes of low and high ESS indicates no difference in low ESS patterns between large LRP and non-large LRP arteries (p = NS) (Supplemental Figure 1). There was a greater total arterial surface area and percentage of arterial surface area of high ESS in large LRP arteries compared with non-large LRP arteries. The frequency distribution of maxPB was significantly higher in larger LRP arteries compared with non-large LRP arteries (Supplemental Figure 2).

3.4. Spatial relationship of local ESS, MaxPB, and MLA relative to site of $maxLCBI_{4mm}$

The location of the $maxLCBI_{4mm}$ was spatially discordant from the site of the MLA ($p < 0.0001$), maxESS ($p = 0.003$), and minESS ($p = 0.003$) in the majority of arteries in both study groups (Fig. 3). There was no difference in the proportion of arteries with concordant $maxLCBI_{4mm}$ and site of the MLA (41% *vs.* 23%; $p = 0.14$), minESS (22% *vs.* 19%; $p = 0.79$), maxESS (41% *vs.* 23%; $p = 0.14$), or maxPB (50% *vs.* 44%, $p = 0.61$) between the large and non-large LRP groups. Consequently, there was no difference in the proportion of arteries with discordant $maxLCBI_{4mm}$ with site of the MLA (59% *vs.* 77%; $p = 0.23$), minESS (78% vs 81%; $p = 0.78$), maxESS (59% vs 77%; $p = 0.23$), or maxPB (50% *vs.* 44%, $p = 0.61$) between the large and non-large LRP groups.

4. Discussion

In a cohort of patients who underwent coronary angiography with simultaneous NIRS-IVUS imaging, there was significant spatial heterogeneity of plaque prognostic characteristics (minESS, maxESS, maxPB, and $maxLCBI_{4mm}$) along the course of each plaque (Graphical abstract), both within and between high-risk characteristics. The maxESS location was most frequently found at, or 3 mm proximal to, the site of the MLA, while the minESS location was not found at the site of the MLA, but equally present proximal and distal to the MLA. MaxPB was primarily located at the MLA, and $maxLCBI_{4mm}$ was found in approximately equal proportions at the site of, distal to, or proximal to the MLA. Furthermore, the locations of the MLA, minESS, and maxESS were spatially discordant from the $maxLCBI_{4mm}$ in

most arteries, independent of the presence of large or non-large LRP. Large LRP arteries had lower minESS and MLA and higher maxESS and maxPB compared with non-large LRP arteries. Thus, arteries with large LRP, which have been shown to be a marker of higher risk patients, more often contain extremes of ESS as well as larger PB and smaller MLA. There was no difference in the arterial area of low ESS between the two groups. However, large LRP arteries had a greater area of high ESS compared with non-large LRP arteries, which is expected since the MLA was significantly smaller in large LRP arteries.

The discordance observed between the locations of the MLA, maxESS, minESS, maxPB, and $maxLCBI_{4mm}$ underscores the heterogeneity of plaque morphology and constituents along the course of individual plaques. This is consistent with findings from prior studies that have utilized virtual histology-IVUS [18,24], radiofrequency-IVUS [11], grey-scale IVUS [10,19] and optical coherence tomography (OCT) [25]. The fact that the site of the MLA was discordant with the majority of potential plaque destabilizing characteristics in the majority of arteries may indicate that plaque progression and destabilization do not occur at the site of the MLA, but proximal or distal to it. Consistent with this concept, a prior IVUS study demonstrated plaque rupture occurred at the site of the MLA in only 16% of culprit lesions. In contrast, the site of plaque rupture was either upstream or downstream from the MLA location in >80% of cases [26].

The findings of the present report may provide important mechanistic insights regarding the recently reported ISCHEMIA trial [27], in which revascularization of severe ischemia-producing MLA obstructions did not reduce death or myocardial infarction in stable CAD patients over a median of 3.2 years. These findings may be explained by the fact that high-risk plaque areas prone to cause MACE may be located heterogeneously along the length of the coronary plaque and not limited to the focal MLA, as indicated by the data in this analysis. However, the MLA may be the area responsible for the presence and severity of ischemia and, therefore, a potential revascularization target. It is likely that PCI directed at the ischemia-producing MLA alone would leave behind adjacent pro-inflammatory and pro-thrombotic plaque areas that remain at high risk of destabilization.

The specific ESS pattern that leads to plaque destabilization remains an active area of investigation. Prior studies have implicated both high ESS [12,26] and low ESS [10,11,20] in plaque destabilization and MACE. The results from the current study show that areas of maxESS and minESS are frequently found adjacent to one another in a given artery, and not necessarily at the site of the $maxLCBI_{4mm}$ or MLA. Given the proximity of high and low ESS areas in the vicinity of an individual plaque, thorough intravascular imaging studies with detailed baseline plaque characterization and follow-up of the culprit location responsible for MACE will be required to discern the subtleties of local ESS environments. This approach may ultimately determine which ESS pattern is responsible for plaque progression and destabilization.

Identification of the detailed ESS nature and location responsible for plaque destabilization is likely very important for accurate prognostication of individual plaques. Due to fundamental fluid dynamics principles, every plaque with a narrow MLA will have associated high ESS at the throat of the obstruction. Depending on the morphology and

slope of the plaque luminal border up- and down-stream from the throat, however, the adjacent low ESS may or may not be low enough to exert a sufficiently intense pro-inflammatory stimulus that may lead to plaque destabilization and MACE [28]. In the Fractional Flow Reserve *versus* Angiography for Multivessel Evaluation 2 (FAME 2) study, only 12.7% of plaques with an abnormally low fractional flow reserve and narrow MLA were associated with a future MACE [29]. It is possible that the minority of plaques with high ESS that destabilize may be those with adjacent low ESS. A recent *post-hoc* analysis of FAME-2 investigating the role of ESS in precipitation of acute MI indicated that high, and not low, ESS was associated with acute MI [12]. It will be necessary to investigate detailed plaque and ESS characteristics in plaques that lead to MACE to understand which variables, and in which locations, are responsible for destabilization.

The ability of NIRS-IVUS imaging to identify high-risk patients and high-risk individual coronary arterial plaques has been evaluated in a prospective manner in the recently published Lipid-Rich Plaque Study [17], which showed that elevated maxLCBI$_{4mm}$ in non-culprit coronary arteries is associated with increase MACE risk on both a patient and plaque level. The Providing Regional Observations to Study Predictors of Events in the Coronary Tree II (PROSPECT II) [30] study will provide additional prospective data regarding the utility of NIRS-IVUS in coronary plaque risk stratification. It will be important to understand the spatial relationships between NIRS-IVUS findings (maxLCBI$_{4mm}$, MLA, PB) and local ESS in plaques that destabilize and cause a new MACE from these natural history studies.

This study has several limitations. First, the limited sample size of 60 arteries was derived from 49 patients, so patients who contributed more than one artery may have biased the results. Second, only arteries that were sufficient for vascular profiling analysis were included in this study, which may have led to selection bias. Third, the study was cross-sectional, so the temporal relationship between ESS pattern, MLA, PB, and maxLCBI$_{4mm}$ cannot be determined. Whether a particular ESS pattern (high or low) that is spatially concordant or discordant with maxLCBI$_{4mm}$ leads to plaque progression or destabilization can be determined only from a study that tracks these variables in patients serially over time. Such efforts may be more feasible using non-invasive imaging modalities, such as coronary computed tomography angiography [15]. Fourth, we measured flows in the coronary arteries excluding side branches. There are evolving techniques that include side branch blood flow, which may provide more accurate local ESS calculations [29]. Lastly, while ESS, MLA, and PB were derived for 3 mm coronary arterial segments, maxLCBI$_{4mm}$ was obtained for 4 mm segments. To maintain consistency with other reports regarding the prognostic role of maxLCBI$_{4mm}$, this metric was used in the present study. Utilization of a 4 mm instead of a 3 mm segment for this variable would not be expected to appreciably influence data interpretation, since there is only one maxLCBI$_{4mm}$ segment within each artery.

In conclusion, the locations of the MLA, minESS, maxESS, and maxPB were spatially discordant from the maxLCBI$_{4mm}$ in the majority of arteries from a cohort of patients who underwent coronary angiography with simultaneous NIRS-IVUS imaging, independent of the presence of large or non-large LRP. The fact that the site of the MLA was discordant with the other high-risk plaque characteristics in the majority of arteries may indicate that

plaque progression and destabilization do not occur at the site of the MLA, but rather either proximal or distal to the MLA. Prospective, longitudinal studies are required to understand which ESS patterns and spatial relationships between plaque elements predict plaque progression and destabilization.

Supplementary Material

Refer to Web version on PubMed Central for supplementary material.

Financial support

This work was supported by Infraredx, Inc. and the Schaubert family.

References

[1]. WHO, Global status report on noncommunicable diseases [Internet]. WHO. [cited 2018 Dec 15]. Available from: http://www.who.int/nmh/publications/ncd-status-report-2014/en/, 2014.

[2]. Siasos G, Tsigkou V, Zaromytidou M, Sara JD, Varshney A, Coskun AU, et al. , Role of local coronary blood flow patterns and shear stress on the development of microvascular and epicardial endothelial dysfunction and coronary plaque, Curr. Opin. Cardiol 33 (6) (2018 Nov) 638–644. [PubMed: 30303854]

[3]. Ford TJ, Berry C, De Bruyne B, Yong ASC, Barlis P, Fearon WF, et al. , Physiological Predictors of acute coronary syndromes: emerging insights from the plaque to the vulnerable patient, JACC Cardiovasc. Interv 10 (24) (2017 Dec 26) 2539–2547. [PubMed: 29268883]

[4]. Stone GW, Maehara A, Lansky AJ, de Bruyne B, Cristea E, Mintz GS, et al. , A prospective natural-history study of coronary atherosclerosis, N. Engl. J. Med 364 (3) (2011 Jan 20) 226–235. [PubMed: 21247313]

[5]. Calvert PA, Obaid DR, O'Sullivan M, Shapiro LM, McNab D, Densem CG, et al. , Association between IVUS findings and adverse outcomes in patients with coronary artery disease: the VIVA (VH-IVUS in Vulnerable Atherosclerosis) Study, JACC Cardiovasc Imaging 4 (8) (2011 Aug) 894–901. [PubMed: 21835382]

[6]. Cheng JM, Garcia-Garcia HM, de Boer SPM, Kardys I, Heo JH, Akkerhuis KM, et al. , In vivo detection of high-risk coronary plaques by radiofrequency intravascular ultrasound and cardiovascular outcome: results of the ATHEROREMO-IVUS study, Eur. Heart J 35 (10) (2014 Mar) 639–647. [PubMed: 24255128]

[7]. Stone PH, Coskun AU, Kinlay S, Popma JJ, Sonka M, Wahle A, et al. , Regions of low endothelial shear stress are the sites where coronary plaque progresses and vascular remodelling occurs in humans: an in vivo serial study, Eur. Heart J 28 (6) (2007 Mar) 705–710. [PubMed: 17347172]

[8]. Papafaklis MI, Takahashi S, Antoniadis AP, Coskun AU, Tsuda M, Mizuno S, et al. , Effect of the local hemodynamic environment on the de novo development and progression of eccentric coronary atherosclerosis in humans: insights from PREDICTION, Atherosclerosis 240 (1) (2015 May) 205–211. [PubMed: 25801012]

[9]. Chatzizisis YS, Coskun AU, Jonas M, Edelman ER, Feldman CL, Stone PH, Role of endothelial shear stress in the natural history of coronary atherosclerosis and vascular remodeling: molecular, cellular, and vascular behavior, J. Am. Coll. Cardiol 49 (25) (2007 Jun 26) 2379–2393. [PubMed: 17599600]

[10]. Stone PH, Saito S, Takahashi S, Makita Y, Nakamura S, Kawasaki T, et al. , Prediction of progression of coronary artery disease and clinical outcomes using vascular profiling of endothelial shear stress and arterial plaque characteristics: the PREDICTION Study, Circulation 126 (2) (2012 Jul 10) 172–181. [PubMed: 22723305]

[11]. Stone PH, Maehara A, Coskun AU, Maynard CC, Zaromitydou M, Siasos G, et al. , Role of low endothelial shear stress and plaque characteristics in the prediction of nonculprit major adverse cardiac events: the PROSPECT study, JACC Cardiovasc Imaging (2017 Sep 15).

[12]. Kumar A, Thompson EW, Lefieux A, Molony DS, Davis EL, Chand N, et al. , High coronary shear stress in patients with coronary artery disease predicts myocardial infarction, J. Am. Coll. Cardiol 72 (16) (2018 Oct 16) 1926–1935. [PubMed: 30309470]

[13]. Torii R, Stettler R, Räber L, Zhang Y-J, Karanasos A, Dijkstra J, et al. , Implications of the local hemodynamic forces on the formation and destabilization of neoatherosclerotic lesions, Int. J. Cardiol 272 (2018 Dec 1) 7–12. [PubMed: 30293579]

[14]. Madder RD, Goldstein JA, Madden SP, Puri R, Wolski K, Hendricks M, et al. , Detection by near-infrared spectroscopy of large lipid core plaques at culprit sites in patients with acute ST-segment elevation myocardial infarction, JACC Cardiovasc. Interv 6 (8) (2013 Aug) 838–846. [PubMed: 23871513]

[15]. Madder RD, Husaini M, Davis AT, VanOosterhout S, Harnek J, Götberg M, et al. , Detection by near-infrared spectroscopy of large lipid cores at culprit sites in patients with non-ST-segment elevation myocardial infarction and unstable angina, Catheter Cardiovasc Interv Off J Soc Card Angiogr Interv 86 (6) (2015 Nov 15) 1014–1021.

[16]. Madder RD, Puri R, Muller JE, Harnek J, Götberg M, VanOosterhout S, et al. , Confirmation of the intracoronary near-infrared spectroscopy threshold of lipid-rich plaques that underlie ST-segment-elevation myocardial infarction, Arterioscler. Thromb. Vasc. Biol 36 (5) (2016 May) 1010–1015. [PubMed: 26941016]

[17]. Waksman R, Mario CD, Torguson R, Ali ZA, Singh V, Skinner WH, et al. , Identification of patients and plaques vulnerable to future coronary events with near-infrared spectroscopy intravascular ultrasound imaging: a prospective, cohort study, Lancet 394 (10209) (2019 Nov 2) 1629–1637. [PubMed: 31570255]

[18]. Brown AJ, Teng Z, Calvert PA, Rajani NK, Hennessy O, Nerlekar N, et al. , Plaque structural stress estimations improve prediction of future major adverse cardiovascular events after intracoronary imaging, Circ Cardiovasc Imaging 9 (6) (2016).

[19]. Antoniadis AP, Papafaklis MI, Takahashi S, Shishido K, Andreou I, Chatzizisis YS, et al. , Arterial remodeling and endothelial shear stress exhibit significant longitudinal heterogeneity along the length of coronary plaques, JACC Cardiovasc Imaging 9 (8) (2016) 1007–1009. [PubMed: 27491487]

[20]. Giannopoulos AA, Zhao S, Chatzizisis YS, Rupture of a stenotic thin-cap fibroatheroma in an area of low endothelial shear stress: implication for mechanism of acute coronary syndromes, Eur Heart J Cardiovasc Imaging 19 (8) (2018 01) 950–951. [PubMed: 29579178]

[21]. Costopoulos C, Maehara A, Huang Y, Brown AJ, Gillard JH, Teng Z, et al. , Heterogeneity of plaque structural stress is increased in plaques leading to MACE: insights from the PROSPECT study, JACC Cardiovasc Imaging 13 (5) (2020 May) 1206–1218. [PubMed: 31326476]

[22]. Madder RD, Khan M, Husaini M, Chi M, Dionne S, VanOosterhout S, et al. , Combined near-infrared spectroscopy and intravascular ultrasound imaging of pre-existing coronary artery stents: can near-infrared spectroscopy reliably detect neoatherosclerosis? Circ Cardiovasc Imaging 9 (1) (2016 Jan).

[23]. Bourantas CV, Papafaklis MI, Athanasiou L, Kalatzis FG, Naka KK, Siogkas PK, et al. , A new methodology for accurate 3-dimensional coronary artery reconstruction using routine intravascular ultrasound and angiographic data: implications for widespread assessment of endothelial shear stress in humans, Eurointervention J Eur Collab Work Group Interv Cardiol Eur Soc Cardiol 9 (5) (2013 Sep) 582–593.

[24]. Costopoulos C, Huang Y, Brown AJ, Calvert PA, Hoole SP, West NEJ, et al. , Plaque rupture in coronary atherosclerosis is associated with increased plaque structural stress, JACC Cardiovasc Imaging 10 (12) (2017) 1472–1483. [PubMed: 28734911]

[25]. Yamamoto E, Siasos G, Zaromytidou M, Coskun AU, Xing L, Bryniarski K, et al. , Low endothelial shear stress predicts evolution to high-risk coronary plaque phenotype in the future: a serial optical coherence tomography and computational fluid dynamics study, Circ Cardiovasc Interv 10 (8) (2017 Aug).

[26]. Lee JM, Choi G, Koo B-K, Hwang D, Park J, Zhang J, et al. , Identification of high-risk plaques destined to cause acute coronary syndrome using coronary computed tomographic angiography and computational fluid dynamics, JACC Cardiovasc Imaging (2018 Mar 14).

[27]. Maron DJ, Hochman JS, Reynolds HR, Bangalore S, O'Brien SM, Boden WE, et al. , Initial invasive or conservative strategy for stable coronary disease, N. Engl. J. Med 382 (15) (2020 09) 1395–1407. [PubMed: 32227755]

[28]. Lee JM, Choi G, Hwang D, Park J, Kim HJ, Doh J-H, et al. , Impact of longitudinal lesion geometry on location of plaque rupture and clinical presentations, JACC Cardiovasc Imaging 10 (6) (2017 Jun) 677–688. [PubMed: 27665158]

[29]. De Bruyne B, Pijls NHJ, Kalesan B, Barbato E, Tonino PAL, Piroth Z, et al. , Fractional flow reserve-guided PCI versus medical therapy in stable coronary disease, N. Engl. J. Med 367 (11) (2012 Sep 13) 991–1001. [PubMed: 22924638]

[30]. PROSPECT II & PROSPECT ABSORB - an Integrated Natural History Study and Randomized Trial. - Full Text View - ClinicalTrials.gov [Internet]. [cited 2019 Jan 10]. Available from:: https://clinicaltrials.gov/ct2/show/NCT02171065.

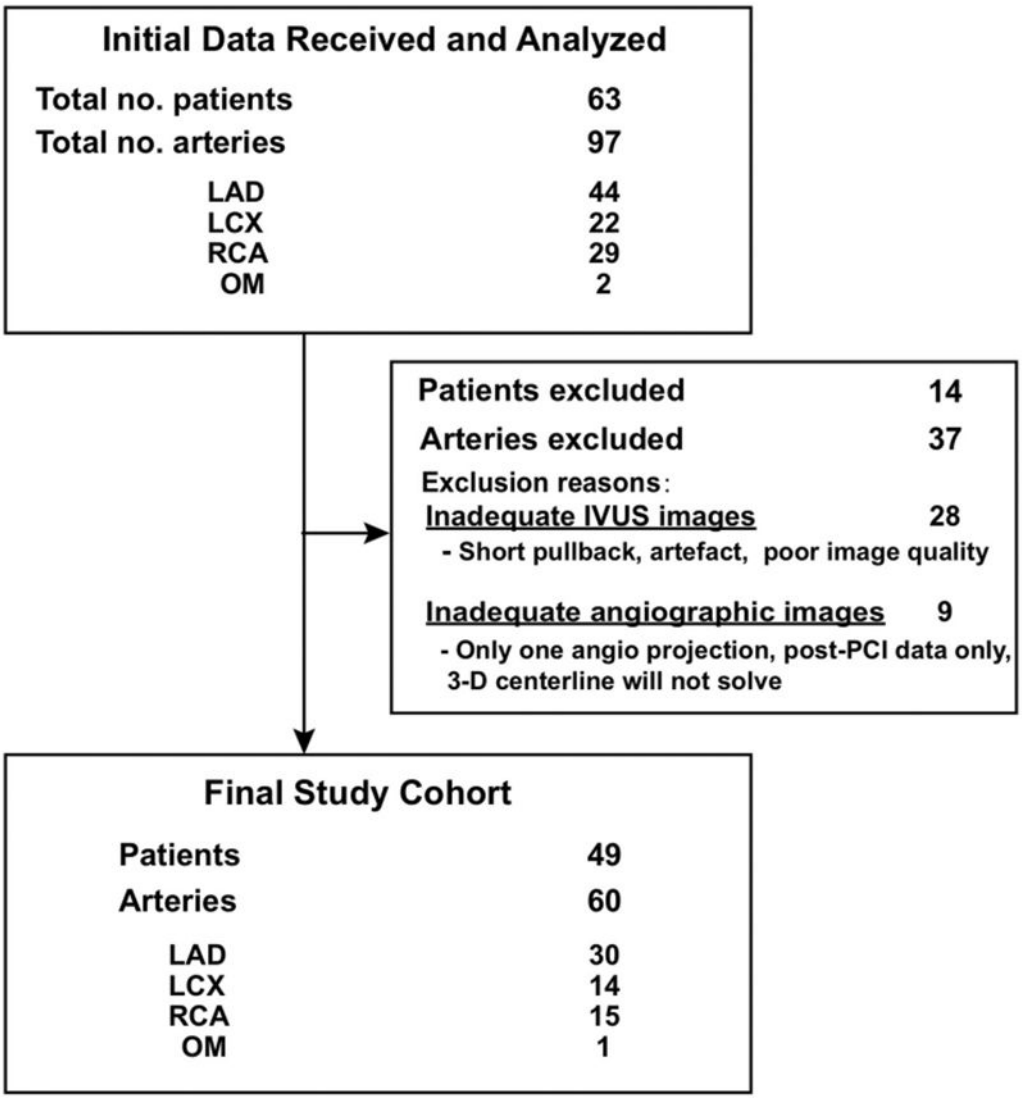

Fig. 1. Study population.

Derivation of analytic study cohort.

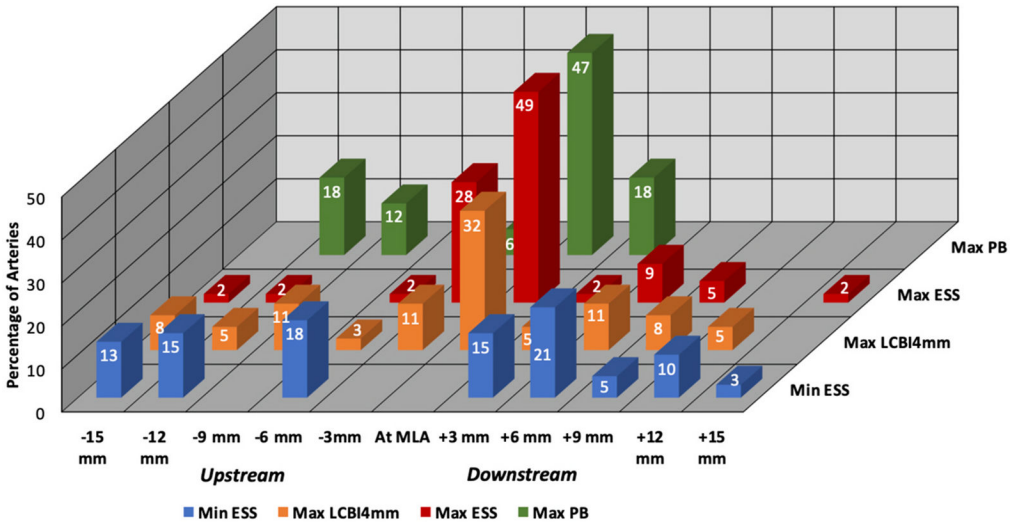

Fig. 2. Spatial distribution of destabilizing features.

Distribution of minESS, maxESS, maxPB, and max$LCBI_{4mm}$, in reference to MLA (n = 58 arteries; 2 arteries with max$LCBI_{4mm}$ of 0 were excluded).

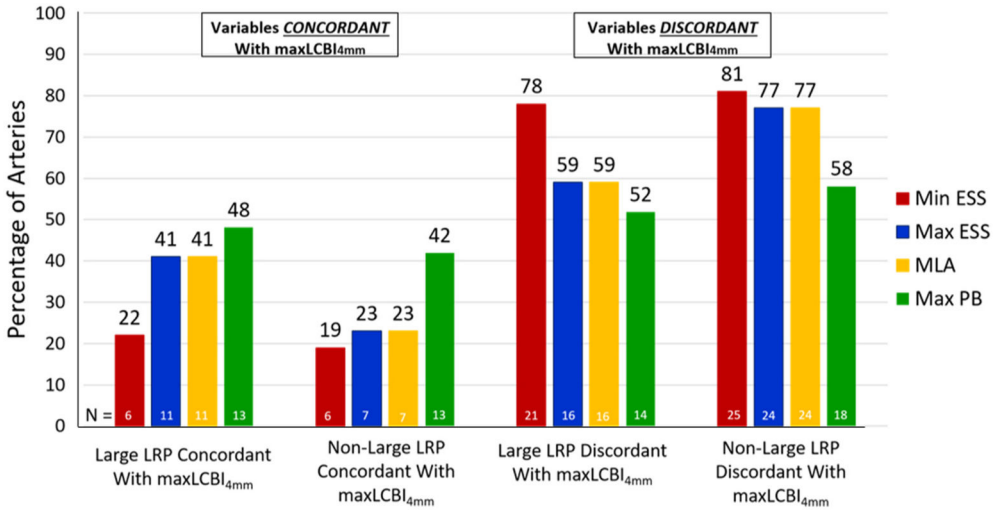

Fig. 3. Spatial concordance and discordance of destabilizing features by study group.

Spatial relationships between location of maxLCBI4mm and sites of minESS, maxESS, maxPB, and MLA by study group (n = 58 arteries; 2 arteries with $maxLCBI_{4mm}$ of 0 were excluded).

Table 1

Patient characteristics.

Baseline characteristics of analytic study cohort.

Age (years)	63.3 ± 10.0
Male sex (%)	33 (67.3%)
Body mass index (kg/m^2)	30.8 ± 6.5
Current smoker (%)	13 (26.5%)
Hypertension (%)	31 (63.3%)
Diabetes mellitus (%)	5 (10.2%)
Hyperlipidemia (%)	30 (61.2%)
Peripheral vascular disease (%)	4 (8.2%)
History of MI (%)	6 (12.2%)
History of PCI (%)	9 (18.4%)
ACS on presentation (%)	17 (34.7%)

Values are mean ± standard deviation or n (%).

ACS, acute coronary syndrome; MI, myocardial infarction; PCI, percutaneous coronary intervention.

Author Manuscript

Author Manuscript

Author Manuscript

Table 2

Arterial characteristics by study group.

Characteristics of large LRP *vs.* non-large LRP arteries.

	Large LRP (n = 27)	**Non-large LRP (n = 33)**	***p*-value**
$maxLCBI_{4mm}$	610.2 ± 161.4	200.1 ± 109.5	<0.0001
Lowest ESS (Pa)	0.41 ± 0.16	0.61 ± 0.36	0.007
Highest ESS (Pa)	9.31 ± 4.78	6.32 ± 5.44	0.023
MLA (mm^2)	3.54 ± 1.22	5.14 ± 2.65	0.002
Max plaque burden (%)	70.64% ± 9.95%	56.70 ± 13.31%	<0.0001
% Area with ESS < 1.0 Pa	20.9% ± 13.8%	26.0% ± 24.9%	0.86
% Area with ESS > 3.5 Pa	35.5% ± 21.9%	19.4% ± 23.8%	0.028
Diameter stenosis (%, median [IQR])	90% (55–99%)	40% (30–60%)	<0.0001

ESS, endothelial shear stress; IQR, interquartile range; LCBI, lipid core burden index; LRP, lipid rich plaque; MLA, minimal luminal area.